Supporting Information

for

One-Pot Synthesized Hierarchical Zeolites Supported Metal Nanoparticles for Highly Efficient Biomass Conversion

Darui Wang, Bing Ma, Bo Wang, Chen Zhao* and Peng Wu*

Shanghai Key Laboratory of Green Chemistry and Chemical Processes, School of Chemistry and Molecular Engineering, East China Normal University, North Zhongshan Rd. 3663, Shanghai 200062, China

EXPERIMENTAL SECTION

Chemicals

All chemicals and reagents were obtained from commercial suppliers and used without further purification: tetraethyl orthosilicate (Sigma-Aldrich, ≥98% Reagent Grade), tetrapropylammonium hydroxide (TCI, 25 wt% in water), colloidal silica (Sigma-Aldrich, 30 wt%), piperidine (Aladdin, ≥99.5% analytical standard), aluminum sulfate octadecahydrate (Aladdin, 98.0%–102.0% ACS reagent), sodium hydroxide (Alfa Aesar, 98.0% flake), ammonium chloride (Alfa Aesar, ≥98%), aqueous ammonia solution (Sinopharm Chemical Reagent Co., Ltd., 28 wt%), $Ni(CH_3COO)_2 \cdot 4H_2O$ (Sinopharm Chemical Reagent Co., Ltd., ≥98% analytical standard), $Cu(CH_3COO)_2 \cdot H_2O$ (Sinopharm Chemical Reagent Co., Ltd., ≥98% analytical standard), $Co(CH_3COO)_2 \cdot 4H_2O$ (Sinopharm Chemical Reagent Co., Ltd., ≥98% analytical standard), $Ni(NO_3)_2 \cdot 6H_2O$ (Sinopharm Chemical Reagent Co., Ltd., ≥98% analytical standard), stearic acid (Sinopharm Chemical Reagent Co., Ltd., analytical standard), *n*-dodecane (Sinopharm Chemical Reagent Co., Ltd., ≥98% GC assay). Air, H_2, and N_2 gases (99.999 vol.%) were supplied by Shanghai Pujiang Specialty Gases Co., Ltd.

Synthesis of ZSM-5 zeolite

ZSM-5 zeolites were synthesized with the assistant of active seeds. The active seeding gel was prepared according to the procedures reported previously.[1] Tetraethyl orthosilicate (TEOS) was dropped into the solution containing water and tetrapropylammonium hydroxide (TPAOH, 25 % aqueous solution). After homogenizing at 353 K for 2 h, the synthetic gel with a molar composition of 1.0 TEOS : 0.15 TPAOH : 14 H_2O was introduced into a Teflon-lined steel autoclave and aged at 393 K for 3 h. After cooling, the obtained seeding gel was directly used for the synthesis of ZSM-5 zeolites without any treatment.

ZSM-5 zeolite was synthesized from piperidine (PI) as structure directing agent, silica sol (30 wt.% SiO_2), aluminum sulfate and sodium hydroxide. Sodium hydroxide and aluminum sulfate were first dissolved in the aqueous solution of piperidine. Silica sol and active seeding gel were then dropped into the above solution and further stirred for 30 minutes, forming a gel composition of 1.0 SiO_2 : 0.0125 Al_2O_3 : 0.2 PI : 0.05 Na_2O : 25 H_2O. SiO_2 in the active seeding gel accounted for 1 % of the whole SiO_2 in gel. The gel was crystallized in a Teflon-lined steel autoclave at 443 K for 72 h. The ZSM-5 product was collected by filtration followed by washing with distilled water several times, dried at 373 K overnight, and then calcined in air at 823 K for 6 h to remove the organic template. The resulting ZSM-5 was brought into ammonium form *via* three consecutive exchanges in 1 M ammonium chloride solution at 353 K for 2 h. After filtration, washing and drying overnight at 373 K, the ammonium ion-exchanged zeolite was subsequently calcined at 823 K for 6 h to give proton-type H-ZSM-5.

Synthesis of nickel silicate precursors coated on ZSM-5 ($NiSiO_2$/ZSM-5)

$NiSiO_2$/ZSM-5 was prepared through a simple hydrothermal process. In a type synthesis, $Ni(CH_3COO)_2 \cdot 4H_2O$ (0.174 g), NH_4Cl (0.749 g) and $NH_3 \cdot H_2O$ (1.274 g, 28%) were added under stirring in 70 g of distilled water. As prepared H-ZSM-5 (ranging from 0.1 g to 0.4 g) was then added to the above solution and ultrasonicated for 30 min to form a uniform suspension, then the mixture was transferred to a Teflon autoclave (100 mL) and heated to 120 ^oC for 3 h. After the autoclave was cooled to room temperature, the resulting green precipitates were collected and washed several times with distilled water and absolute ethanol. The final products were dried under vacuum at 60 ^oC for 4 h.

Synthesis of nickel nanoparticles supported on ZSM-5 (Ni/ZSM-5)

$NiSiO_2$/ZSM-5 was placed in a quartz boat in the middle of the horizontal tube furnace. After decomposition and reduction under a H_2 flow (flow rate: 100 mL min^{-1}) at 550 ^oC for 5 h with a heating rate of 2 ^oC min^{-1}, black power of Ni/ZSM-5 was collected in the quartz boat at room temperature.

Synthesis of copper nanoparticles and cobalt nanoparticles supported on ZSM-5

(Cu/ZSM-5 and Co/ZSM-5)

Cu/ZSM-5 and Co/ZSM-5 were prepared under a similar experimental process by varying the corresponding metallic salt and experimental temperature.

Copper silicate precursors ($CuSiO_2$/ZSM-5) were prepared under hydrothermal condition at 150 ^oC for 3 h, then Cu/ZSM-5 was obtained by decomposition and reduction of $CuSiO_2$/ZSM-5 under a H_2 flow at 350 ^oC for 5 h.

Cobalt silicate precursors ($CoSiO_2$/ZSM-5) were prepared under hydrothermal condition at 100 ^oC for 3 h, then Co/ZSM-5 was obtained by decomposition and reduction of $CoSiO_2$/ZSM-5 under a H_2 flow at 450 ^oC for 5 h.

Synthesis of IM-Ni/ZSM-5 by wetness impregnation method

In a typical synthesis, $Ni(NO_3)_2$ $6H_2O$ (ranging from 0.372 g to 1.487 g) was dissolved in distilled water (1 g), and then the solution was slowly dropped onto H-ZSM-5 zeolite (1 g) with continuous stirring at ambient temperature for a total of 4 h. After completing this procedure, the material was firstly dried overnight at ambient temperature and then further at 110 ^oC for 12 h. Afterwards, the catalyst precursor was calcined in air (flow rate: 100 mL min^{-1}) at 400 ^oC for 4 h and reduced under a H_2 flow (flow rate: 100 mL min^{-1}) at 500 ^oC for 5 h with a heating rate of 2 ^oC min^{-1}.

Catalytic reactions

In a typical test, stearic acid (5.0 g), dodecane (80 mL), and Ni/ZSM-5 catalyst (0.2 g) were charged into a batch autoclave (Parr Instrument, 300 mL). The reactor was then flushed with N_2 for three times in order to remove the residual air; afterwards H_2 gas (4 MPa) was introduced into the reactor when the temperature reached 260 ℃. The reaction was conducted for 60 min

at a stirring speed of 600 rpm. During the reaction, the liquid products were collected by sampling every 20 min interval, and subsequently analyzed by gas chromatography-mass spectroscopy (Techcomp 7900) equipped with a Rtx-5Sil MS capillary column (30 m × 0.25 mm × 0.25 μm). Undecane was used as an internal standard to calculate the yields of liquid products. Analysis for gaseous products was performed on a GC (Techcomp 7900) equipped with a TCD and two columns (TDX-01: 30 cm × 3 mm, TDX-01: 2 m × 3 mm). Conversion = (weight of converted reactant)/(weight of the starting reactant) × 100%. Yield of liquid products = (C atoms in liquid products/C atoms in the starting reactant) × 100%.

For catalyst recycle, the catalysts were separated by centrifugation, washed with acetone to remove organics, dried in ambient air at 60 ^{o}C overnight, and then activated again in H_2 carrier gas at 550 ^{o}C for 4 h. Without other treatments, the Ni catalyst was reused in the next catalytic run.

Characterization methods

Powder X-ray diffraction (XRD) was employed to check the structure and crystallinity of the zeolites. The XRD patterns were collected on a Rigaku Ultima IV diffractometer using Cu Kα radiation at 35 kV and 25 mA in the 2θ angle range of 5 - 80 ^{o}using a step size of 0.02 °and at a scanning speed of 10 °min^{-1}.

Nitrogen gas adsorption measurements were carried out at 77 K on a BEL-MAX gas/vapor adsorption instrument. The samples were evacuated at 573 K for at least 6 h before adsorption. The *t*-plot method was used to discriminate between micro- and mesoporosity. The surface areas were calculated by the Brunauer-Emmett-Teller (BET) method. The mesopore size distribution was obtained by the BJH model from the adsorption branches of the isotherms.

Si, Ni and Al contents were determined by inductively coupled plasma emission spectrometry (ICP) on a Thermo IRIS Intrepid II XSP atomic emission spectrometer.

The IR spectra were collected on a Nicolet Nexus 670 FT-IR spectrometer in absorbance mode at a spectral resolution of 2 cm^{-1} using KBr technique (2 wt% wafer).

The pyridine-adsorption FI-IR spectra were also collected on a Nicolet Nexus 670 FT-IR spectrometer in absorbance mode at a spectral resolution of 2 cm^{-1}. The sample was pressed into a self-supported wafer with 4.8 mg cm^{-2} thickness, which was set in a quartz cell sealed

with CaF_2 windows and connected to a vacuum system. After evacuated at 723 K for 2 h, pyridine adsorption was carried out by exposing the pretreated wafer to a pyridine vapor at 298 K for 0.5 h. The adsorbed pyridine was evacuated successively at 423 K for 1 h. The spectra were collected at room temperature.

Scanning electron microscopy (SEM) was performed on a Hitachi S-4800 microscope to determine the crystal morphology.

Transmission electron microscopy (TEM) images were collected on a Tecnai G^2 F30 microscope. The sample was firstly made suspension in ethanol by ultrasonication, and a drop of such suspension was deposited onto a holey carbon foil supported on a copper grid. More than 300 particles were counted for the histograms of particle size distribution.

The temperature-programmed reduction (TPR) measurement was performed on a self-constructed instrument, by using a stream of 3 % H_2/He mixture and a heating rate of 5 $^oC\ min^{-1}$. The H_2O formation during the TPR experiments was monitored by mass spectrometry.

For determination of metal dispersion, pulse CO chemisorption was tested on a Micromeritics AutoChem 2910. Prior to test, 50 mg catalyst was reduced in a flow of 100 mL min^{-1} 10 vol% H_2 in He at 550 ^oC for 2 h and then flushed in He for 1h. After cooled to ambient temperature in He, the CO gas pulses (5 vol% in He) were introduced in a flow of 100 mL min^{-1}. The changes in the CO gas phase concentration were tracked by TCD.

Table S1 The textural properties of the pristine ZSM-5, treated ZSM-5 and Ni/ZSM-5 with different Ni contents.

Catalyst	S_{BET}[a] ($m^2 g^{-1}$)	S_{ext}[b] ($m^2 g^{-1}$)	V_{tot}[c] ($cm^3 g^{-1}$)	V_{micro}[b] ($cm^3 g^{-1}$)	V_{meso}[d] ($cm^3 g^{-1}$)
Pristine ZSM-5	425	25	0.25	0.17	0.08
Treated ZSM-5[e]	432	28	0.26	0.17	0.09
Ni/ZSM-5 (7.6 wt%)[f]	398	99	0.34	0.13	0.21
Ni/ZSM-5 (10.3 wt%)	384	102	0.37	0.13	0.24
Ni/ZSM-5 (20.4 wt%)	350	104	0.41	0.11	0.30
Ni/ZSM-5 (30.6 wt%)	327	126	0.38	0.09	0.29

[a] Obtained by BET method.

[b] Obtained by *t*-plot method.

[c] Given by the adsorption amount at $P/P_0 = 0.99$.

[d] $V_{meso} = V_{tot} - V_{micro}$.

[e] Treated ZSM-5 was obtained under similar conditions as $NiSiO_2$/ZSM-5 without using Ni source.

[f] The numbers in parentheses indicate the Ni contents actually loaded as analyzed by ICP.

Table S2 The textural properties of IM-Ni/ZSM-5 prepared by wetness impregnation method with different Ni contents.

Catalyst	S_{BET}[a] ($m^2 g^{-1}$)	S_{ext}[b] ($m^2 g^{-1}$)	V_{tot}[c] ($cm^3 g^{-1}$)	V_{micro}[b] ($cm^3 g^{-1}$)	V_{meso}[d] ($cm^3 g^{-1}$)
IM-Ni/ZSM-5 (7.5 wt%)[e]	363	31	0.26	0.15	0.11
IM-Ni/ZSM-5 (10.2 wt%)	344	29	0.25	0.15	0.10
IM-Ni/ZSM-5 (20.2 wt%)	320	28	0.23	0.13	0.10
IM-Ni/ZSM-5 (30.3 wt%)	308	27	0.23	0.12	0.11

[a] Obtained by BET method.

[b] Obtained by *t*-plot method.

[c] Given by the adsorption amount at $P/P_0 = 0.99$.

[d] $V_{meso} = V_{tot} - V_{micro}$.

[e] The numbers in parentheses indicate the Ni contents actually loaded as analyzed by ICP.

Table S3 Characteristic properties of Ni/ZSM-5 and IM-Ni/ZSM-5 catalysts, and their catalytic properties for stearic acid hydrodeoxygenation.[a]

Catalyst	Ni loading[b] (wt%)	d_{Ni}[c] (nm)	D_{Ni}[d] (%)	Rate (mmol g^{-1} h^{-1})	TOF[e] (mol mol^{-1} h^{-1})
Ni/ZSM-5	7.6	5.1 ±1.5	6.1	34	436
Ni/ZSM-5	10.3	5.2 ±1.7	6.0	44	416
Ni/ZSM-5	20.4	5.5 ±1.6	5.4	69	367
Ni/ZSM-5	30.6	6.0 ±1.5	5.0	76	290
IM-Ni/ZSM-5	20.2	30 ±11	2.0	19	282

[a] Reaction conditions: 5.0 g stearic acid, 0.2 g catalyst, 80 mL dodecane, 260 ^{o}C, 4 MPa H_2, 60 min, stirring at 600 rpm.

[b] Ni contents were analyzed by ICP.

[c] Determined by HRTEM.

[d] Calculated by CO chemisorption.

[e] TOF is defined as per mol of consumed reactant per accessible Ni atom per hour.

Table S4 Comparison of stearic acid conversions on Ni/Zeolites prepared by the novel method.[a]

Catalyst	Ni loading[b]	Conv.	Yield (%)			
	(wt%)	(%)	*n*-C17	*iso*-C18	*n*-C18	C18-OH
Ni/ZSM-5	20.4	78.1	9.0	3.8	65.0	0.3
Ni/MOR	20.2	41.0	8.2	0.3	6.4	26.1
Ni/Beta	20.2	70.3	7.6	9.9	50.6	2.2
Ni/HY	20.0	64.8	9.7	1.0	53.5	0.6
Ni/MCM-22	20.1	60.1	7.9	5.6	43.3	3.3

[a] Reaction conditions: 5.0 g stearic acid, 0.2 g catalyst, 80 mL dodecane, 260 ^{o}C, 4 MPa H_2, 60 min, stirring at 600 rpm.

[b] Ni contents were analyzed by ICP.

From the above table, we can see different Ni-containing zeolites showed different stearic acid conversion and product selectivity. Ni/ZSM-5 had the highest stearic acid conversion of 78.1% and *n*-C18 selectivity of 65.0%. Ni/Beta showed the stearic acid conversion of 70.3% and the highest *iso*-C18 selectivity of 9.9%, this result may be due to the 12-membered-ring pores. Because the limited one dimensional pores, Ni/MOR showed the lowest stearic acid conversion of 41.0% and the highest C18-OH selectivity of 26.1%, this meant acid sites in MOR were hard to contact with reactant.

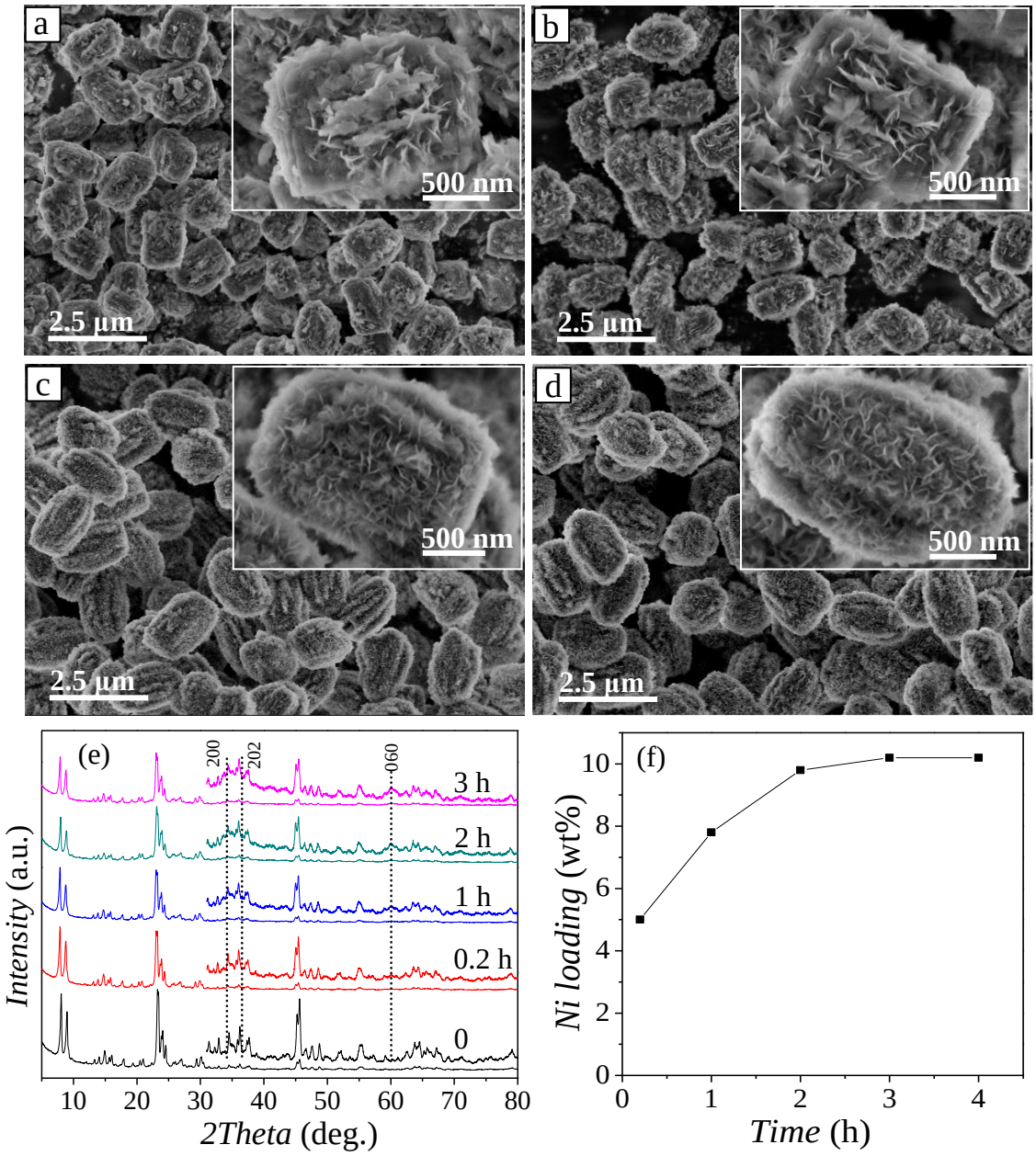

Fig. S1 SEM images of $NiSiO_2$/ZSM-5 collected at different reaction time: 0.2 h (a), 1 h (b), 2 h (c) and 3 h (d); corresponding XRD patterns of $NiSiO_2$/ZSM-5 obtained at different reaction time (e); change of Ni loading (given by ICP analyses) with reaction time (f). The reaction was performed at the temperature of 120 ^oC.

To investigate the effect of reaction time on the loading of Ni and the formation of hierarchical $NiSiO_2$/ZSM-5 composite materials, we monitored the reactions at the same temperature of 120 ^oC but changing the reaction time. At reaction time of 0.2 h, only a small

amount of flower-like nanosheets were coated on the ZSM-5, and about 5.0 wt% Ni was loaded. As the reaction time was extended to 1 h, more flower-like nanosheets emerged. From 2 h to 3 h, no significant change in morphology was observed. The Ni loading was leveled off at 3 h, suggesting that the reaction was complete. The maximum loading of 10 wt% was close to the amount of Ni source added. In XRD patterns, the intensity of peaks indexed as nickel silicate increased with prolonging reaction time, while the intensity of peaks due MFI zeolite topology decreased.

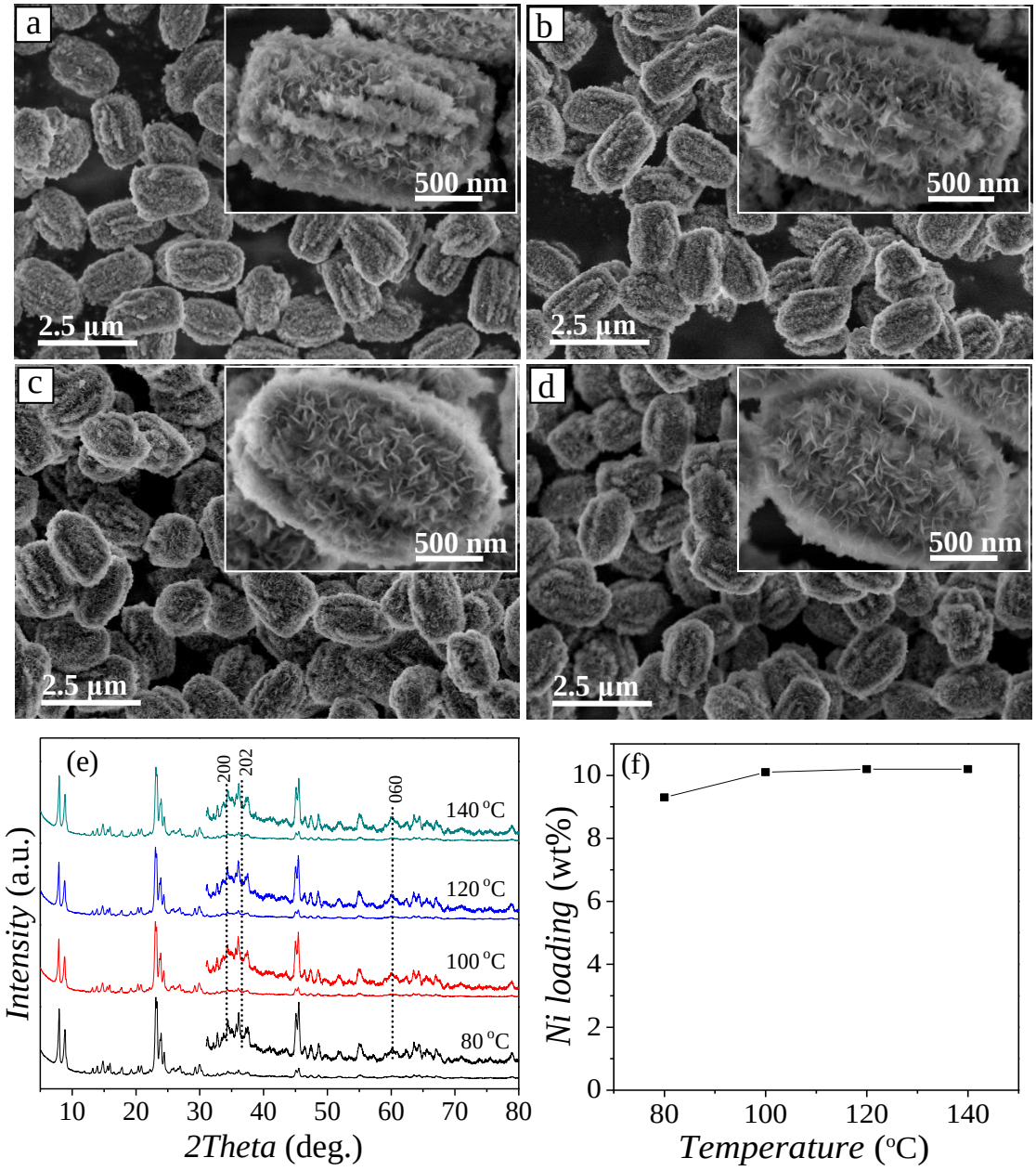

Fig. S2 SEM images of $NiSiO_2$/ZSM-5 obtained at different temperature: 80 °C (a), 100 °C (b), 120 °C (c) and 140 °C (d); corresponding XRD patterns of $NiSiO_2$/ZSM-5 (e); and change of Ni loading (given by ICP analyses) with reaction temperature (f). The reaction was performed for 3 h at different temperatures.

The morphology of $NiSiO_2$/ZSM-5 was significantly affected by reaction temperature. At lower temperatures of 80 °C and 100 °C, the flower-like nanosheets were shorter, tighter and closely aggregated each other. At higher temperatures of 120 °C and 140 °C, the nanosheets

exhibited a much clearer morphology, and became less aggregated. After reduction, the Ni NPs supported on nanosheets are expected to be harder to aggregate according to Ostwald ripening.[2] The XRD patterns and Ni loading did not show significant changes when varying the reaction temperature. Combining these results with those shown in Fig. S1 (ESI†), we deem likely that well-structured $NiSiO_2$/ZSM-5 materials can be prepared by hydrothermal reaction under optimal temperature and time of 120 ^oC and 3 h, respectively.

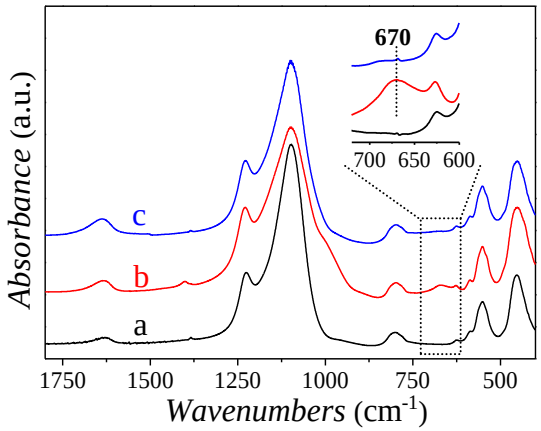

Fig. S3 FT-IR spectra of the pristine ZSM-5 (a), $NiSiO_2$/SM-5 (b) and Ni/ZSM-5 (c). The inset shows the enlarged region for Si-O-Ni stretching vibration.

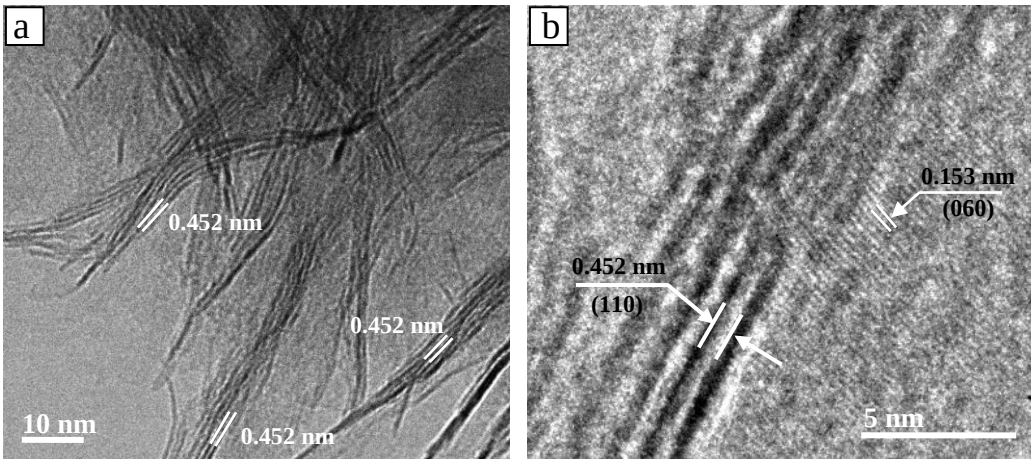

Fig. S4 HRTEM images of flower-like nanosheets. The distance of the adjacent lattice fringes was determined to be about 0.452 nm and 0.153 nm, corresponding well to the d_{110} and d_{060} spacing of $Ni_3Si_2O_5(OH)_4$ (JCPDS No. 49-1859), respectively.

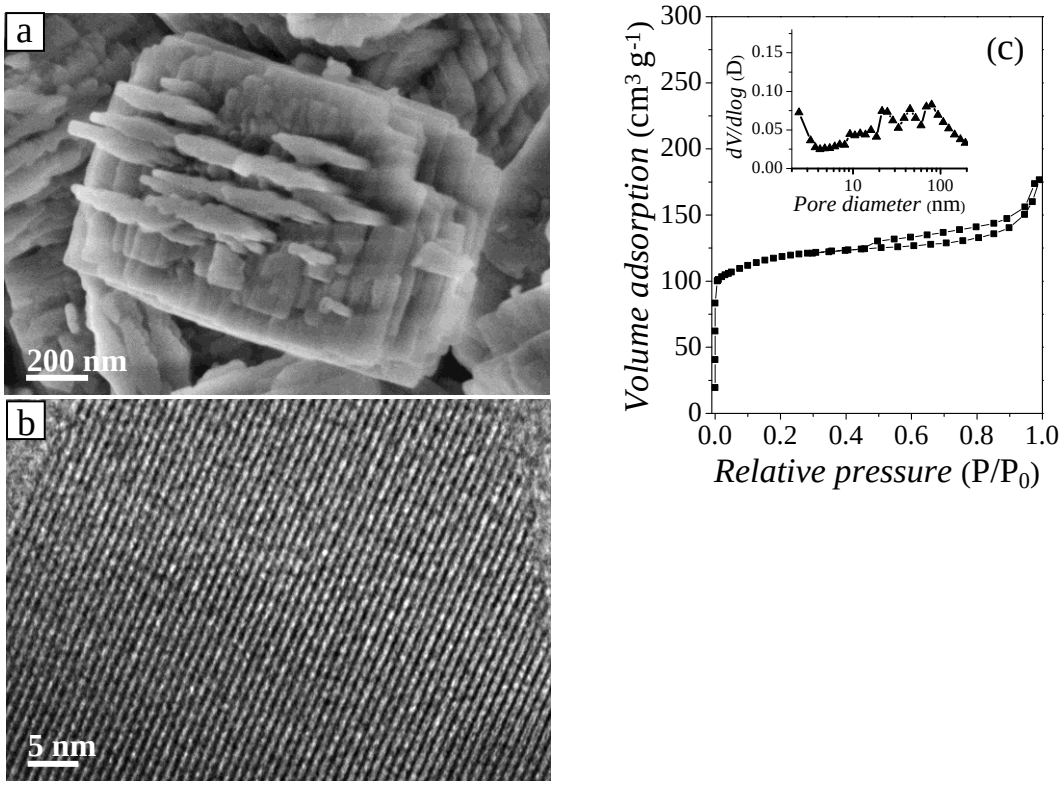

Fig. S5 SEM image (a), TEM image (b) and N_2 isotherm and BJH pore size distribution (c) of the treated ZSM-5.

From the SEM image, we can see the treated ZSM-5 showed the same crystal shape and size as the pristine ZSM-5. TEM image showed that the treated ZSM-5 displayed an ordered arrangement of micropores without interruption in a wide area. N_2 isotherm and BJH pore size distribution also showed the microporous characteristics of the treated ZSM-5 (detailed textural properties can be seen in Table S1), which means that the silica was not extracted from the ZSM-5 crystals during hydrothermal treatment without using Ni source. Compared with the hydrothermal treatment with using Ni source, the addition of Ni source can enhance the rate of silica dissolution. The similar results had been reported by d'Espinose de la Caillerie *et al.*[3] Then layered nickel silicate can be formed through the hydrothermal reaction between silica and Ni^{2+} on the surface of ZSM-5 crystals. Therefore, we can indicate that the micropore part is limited to the core and the mesopore part to the shell of the $NiSiO_2$/ZSM-5.

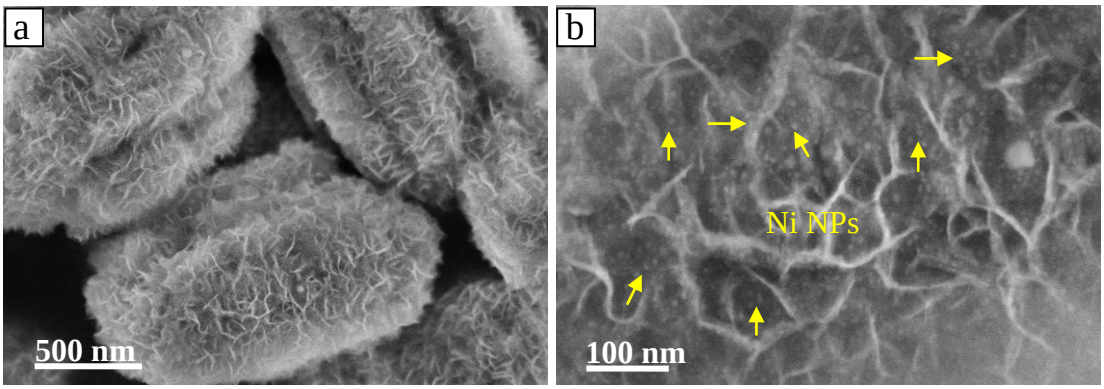

Fig. S6 SEM images of the reduced sample of Ni/ZSM-5 (a, b). From the left image, we can see the core-shell structure was well maintained after decomposition and reduction and there were still flower-like nanosheets coating on the ZSM-5 crystals. In the right image, Ni nanoparticles (bright dots) were uniformly dispersed, having an average particle size of about 5 nm.

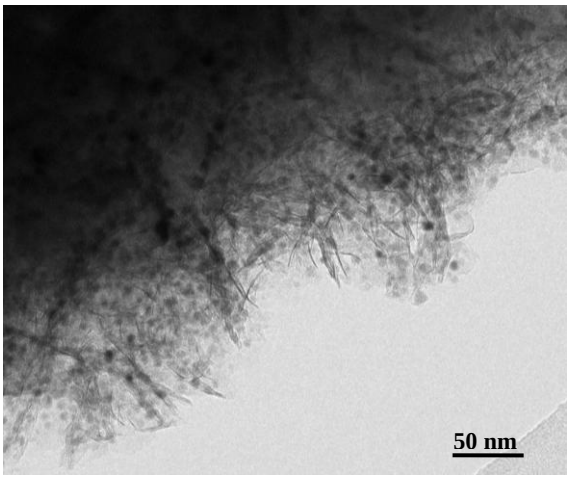

Fig. S7 TEM image of the reduced sample of Ni/ZSM-5. Uniform Ni nanoparticles were dispersed on the SiO_2 matrix, just like "diamond on the beach". Ni nanoparticles are expected to be more stable when located between two adjoining flower-like SiO_2 matrix, then aggregation and leaching can be avoided during reaction at high temperature. This unique distribution pattern of metal NPs are expected to lead to a high activity and stability during reaction.

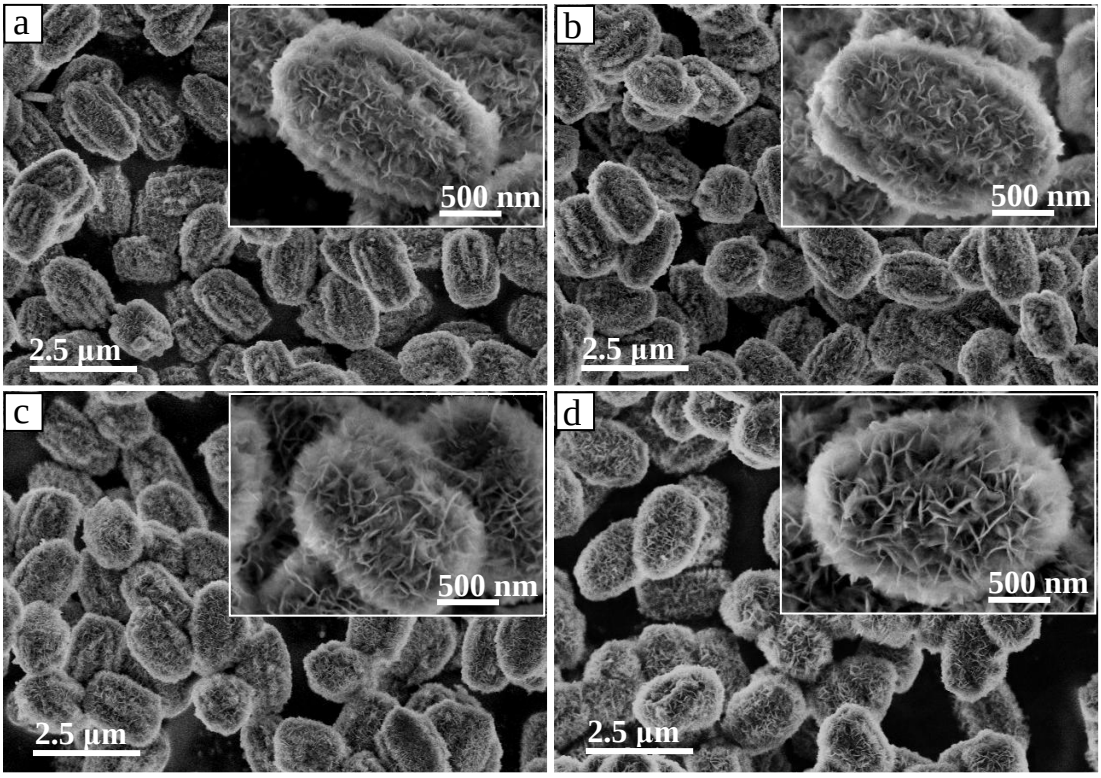

Fig. S8 SEM images of $NiSiO_2$/ZSM-5 with a nickel loading of 7.6 wt% (a), 10.3 wt% (b), 20.4 wt% (c) and 30.6 wt% (d). Nickel contents were determined by ICP analyses. A larger amount of flower-like nanosheets were obtained with an increasing nickel content.

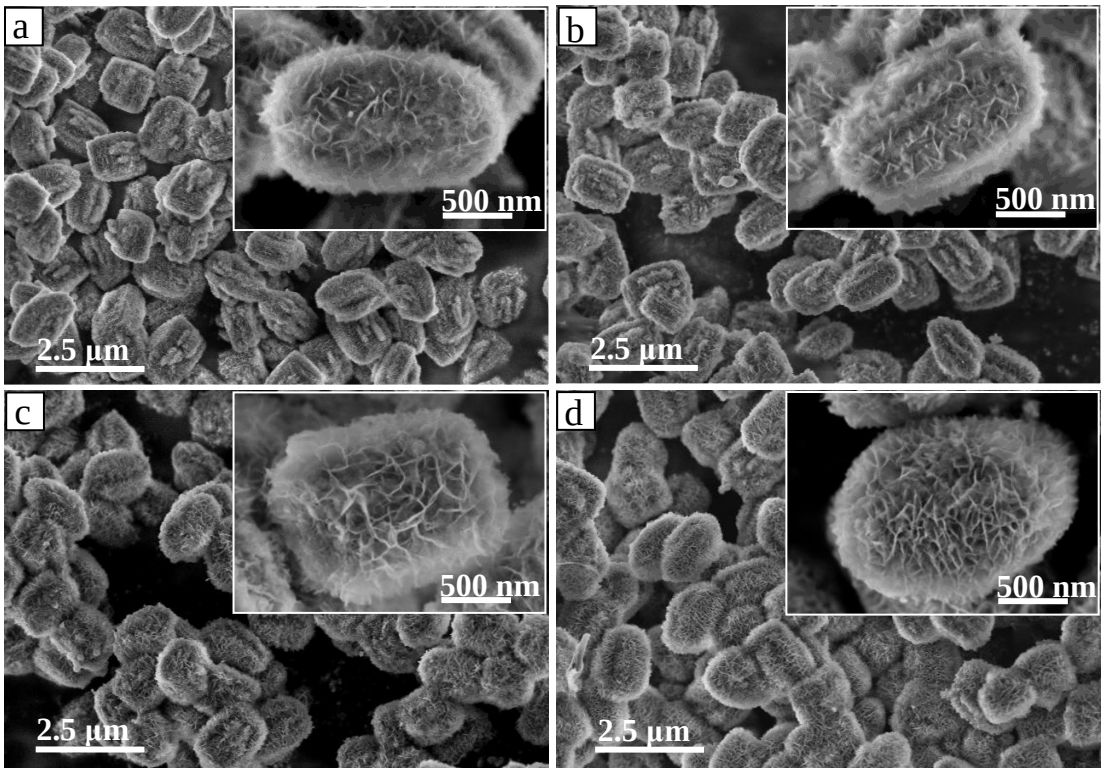

Fig. S9 SEM images of Ni/ZSM-5 with a nickel loading of 7.6 wt% (a), 10.3 wt% (b), 20.4 wt% (c) and 30.6 wt% (d). Ni/ZSM-5 was obtained by decomposition and reduction of $NiSiO_2$/ZSM-5 shown in Fig. S8. After decomposition and reduction, the remaining SiO_2 matrix served as supporter for Ni nanoparticles, and the amount of remaining SiO_2 matrix increased with an increasing nickel content.

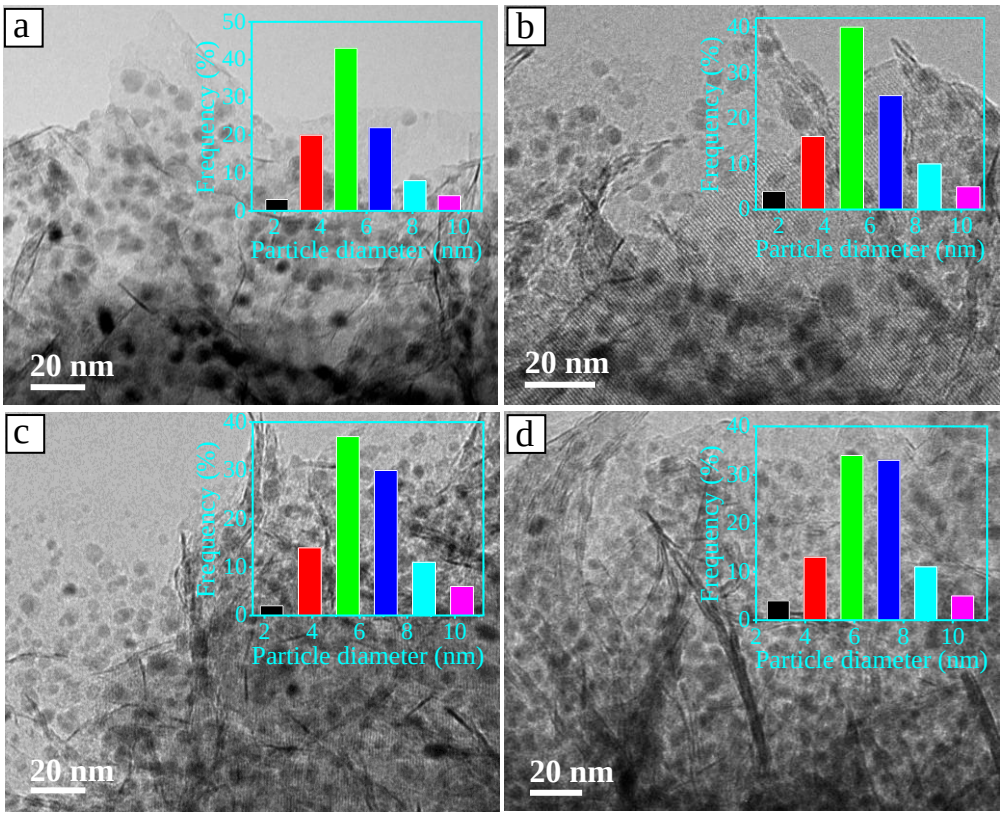

Fig. S10 High-resolution TEM images, corresponding Ni NPs size distribution histogram of Ni/ZSM-5 with a Ni loading of 7.6 wt% (a), 10.3 wt% (b), 20.4 wt% (c) and 30.6 wt% (d).

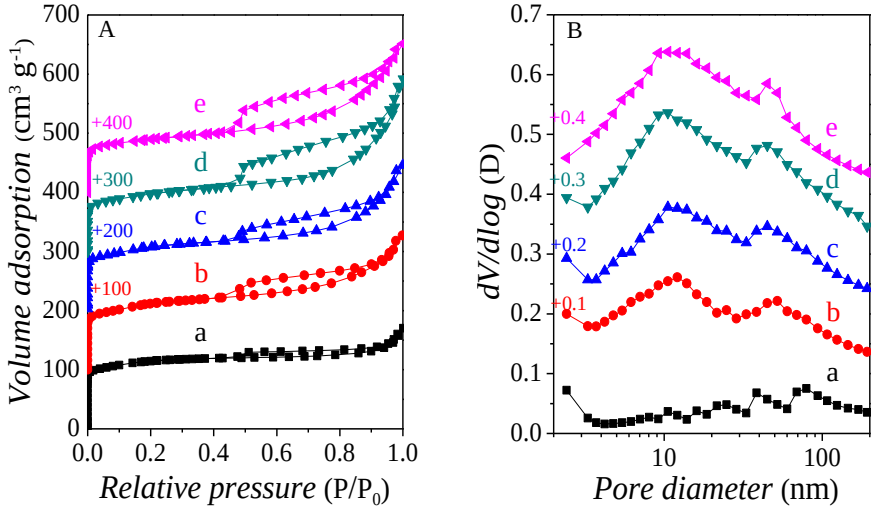

Fig. S11 N_2 isotherms (A) and BJH pore size distributions (B) of pristine ZSM-5 (a) and Ni/ZSM-5 with a Ni loading of 7.6 wt% (b), 10.3 wt% (c), 20.4 wt% (d) and 30.6 wt% (e). Ni contents were analyzed by ICP.

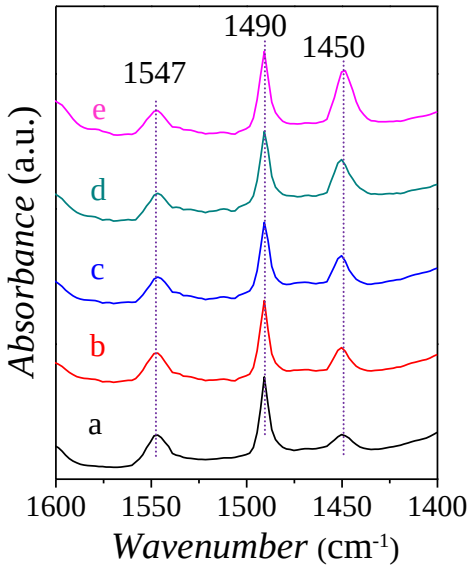

Fig. S12 Pyridine-adsorption FT-IR spectra of pristine ZSM-5 (a) and Ni/ZSM-5 with a nickel content of 7.6 wt% (b), 10.3 wt% (c), 20.4 wt% (d) and 30.6 wt% (e). The spectra were taken on proton-form samples after desorption of pyridine at 150 ^{o}C for 1 h. The stretching bands of at around 1450 and 1547 cm^{-1} were attributed to Lewis acid sites and Brønsted acid sites, respectively.[4]

Compared with ZSM-5, the Ni/ZSM-5 catalysts prepared by the novel method possessed slightly lower concentrations of Brønsted acid sites, possible due to a partial sacrificing and dissolving of the crystalline structure of ZSM-5 during the hydrothermal reaction step in weak alkaline solution. In addition, the concentrations of Lewis acid sites gradually increased with an increasing Ni loading in Ni/ZSM-5. These Ni-based samples still had unreduced ionic Ni species as evidenced by H_2-TPR investigation (Fig. S13, ESI †), which are speculated to be the potential Lewis acid sites.

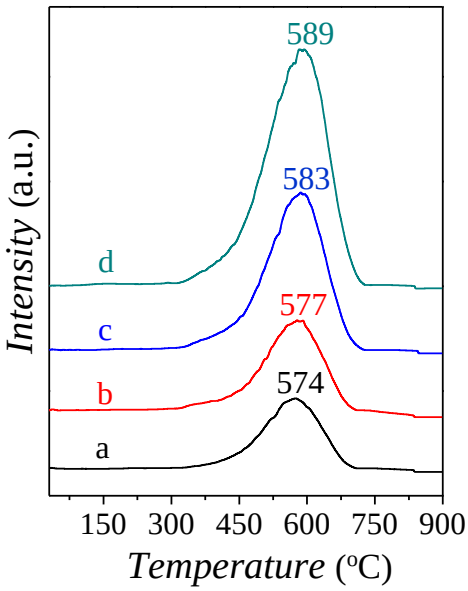

Fig. S13 H_2-TPR profiles of $NiSiO_2$/ZSM-5 precursors with a nickel loading of 7.6 wt% (a), 10.3 wt% (b), 20.4 wt% (c) and 30.6 wt% (d).

The TPR profiles showed broad peaks with maxima at 570 - 590 °C, indicating a strong interaction between nickel and zeolite support. The maxima showed a slight increase when the Ni content increased from 7.6 to 30.6 wt%, probably because the more mesophase SiO_2 formed would strengthen the interaction of Ni NPs with the zeolite support.

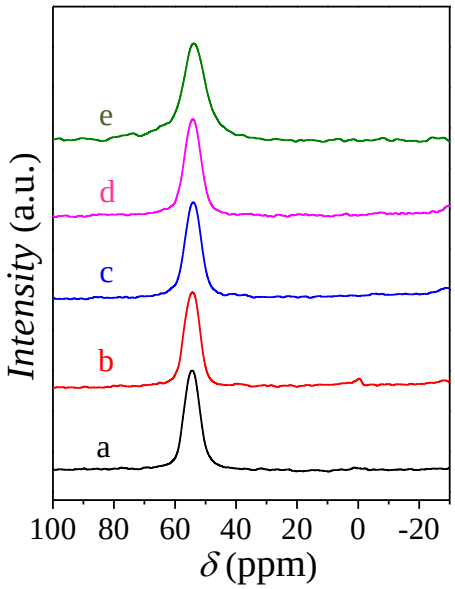

Fig. S14 ^{27}Al MAS NMR spectra of the pristine ZSM-5 (a) and $NiSiO_2$/ZSM-5 precursors with a nickel loading of 7.6 wt% (b), 10.3 wt% (c), 20.4 wt% (d) and 30.6 wt% (e).

The ^{27}Al MAS NMR spectra of the pristine ZSM-5 showed only one signal of tetrahedral Al at 58 ppm, but no resonance at 0 ppm due to octahedral Al, which means that the Al ions were incorporated predominantly in the framework position. After incorporating nickel content, $NiSiO_2$/ZSM-5 precursors also showed only one signal of tetrahedral Al at 58 ppm as pristine ZSM-5, but the signal became broader with the increased nickel content. This implied that the microenvionment of Al became more asymmetrc in coordination states. According to the ICP analyses, the Si/Al molar ratios for the pristine ZSM-5 and $NiSiO_2$/ZSM-5 precursors with a nickel loading of 7.6 wt%, 10.3 wt%, 20.4 wt% and 30.6 wt% were 40.5, 40.8, 40.9, 40.2 and 41.0, respectively. According to the unchanged Si/Al ratio and above broadened signal, we can assume that Al was also extracted from ZSM-5 along with the silica dissolution and Al was incorporated into the nickel slical phase.

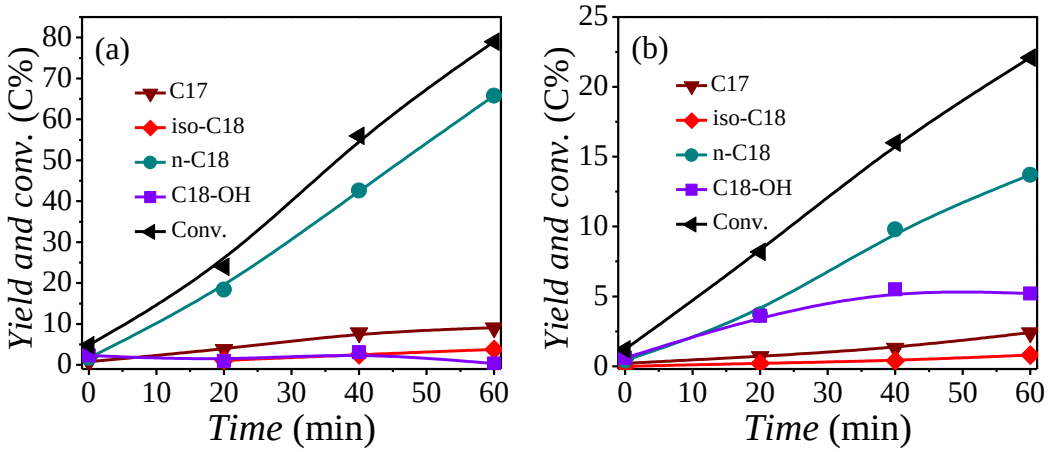

Fig. S15 The kinetics of stearic acid hydrodeoxygenation over Ni/ZSM-5 (20.4 wt% Ni loading) (a) and IM-Ni/ZSM-5 (20.2 wt% Ni loading) (b). Reaction conditions: 5.0 g stearic acid, 0.2 g catalyst, 80 mL dodecane, 260 ^{o}C, 4 MPa H_2, stirring at 600 rpm.

The conversions of stearic acid were 78.1% and 22.1% at 60 min, and the corresponding initial reaction rates were 66 and 19 mmol g^{-1} h^{-1} for Ni/ZSM-5 and IM-Ni/ZSM-5, respectively.

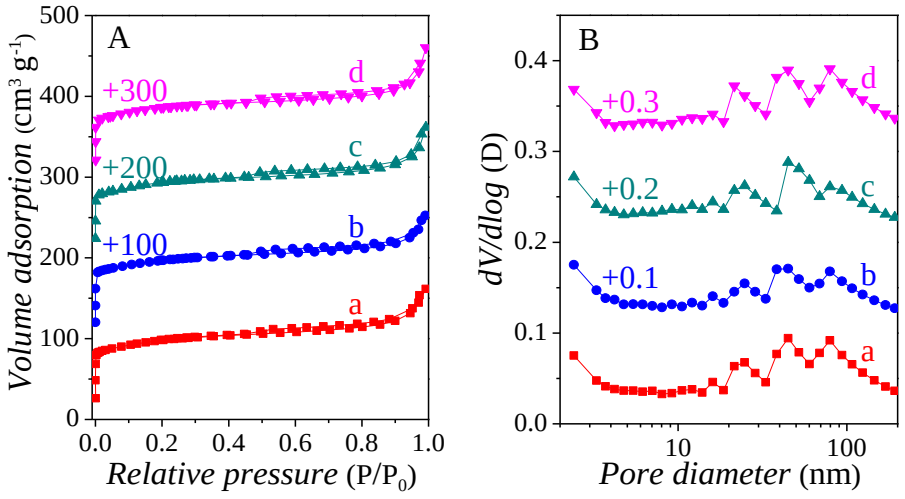

Fig. S16 N_2 isotherms (A) and BJH pore size distributions (B) of IM-Ni/ZSM-5 prepared by wetness impregnation method with a nickel content of 7.5 wt% (a), 10.2 wt% (b), 20.2 wt% (c) and 30.3 wt% (d). Ni contents were analyzed by ICP.

All samples presented a type I isotherm of N_2 adsorption, which is a characteristic of microporosity. The pore size distribution derived from adsorption data and calculated from BJH method indicated that no meopores were produced after loading Ni particles on ZSM-5 using wetness impregnation method. The detailed data of the textural properties are presented in Table S2 (ESI†).

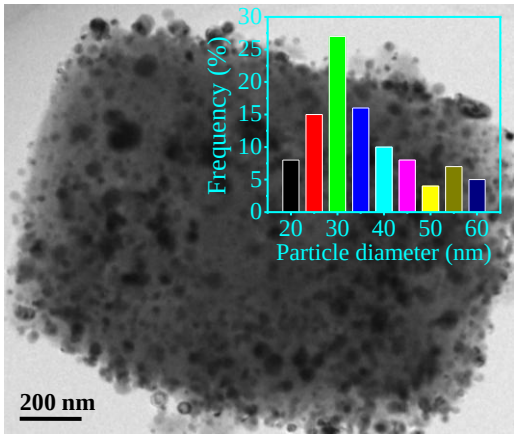

Fig. S17 TEM image of IM-Ni/ZSM-5 (20.2 wt% Ni loading) after calcination and reduction prepared by wet impregnation method. Inset is the corresponding size distribution histogram of the Ni nanoparticles.

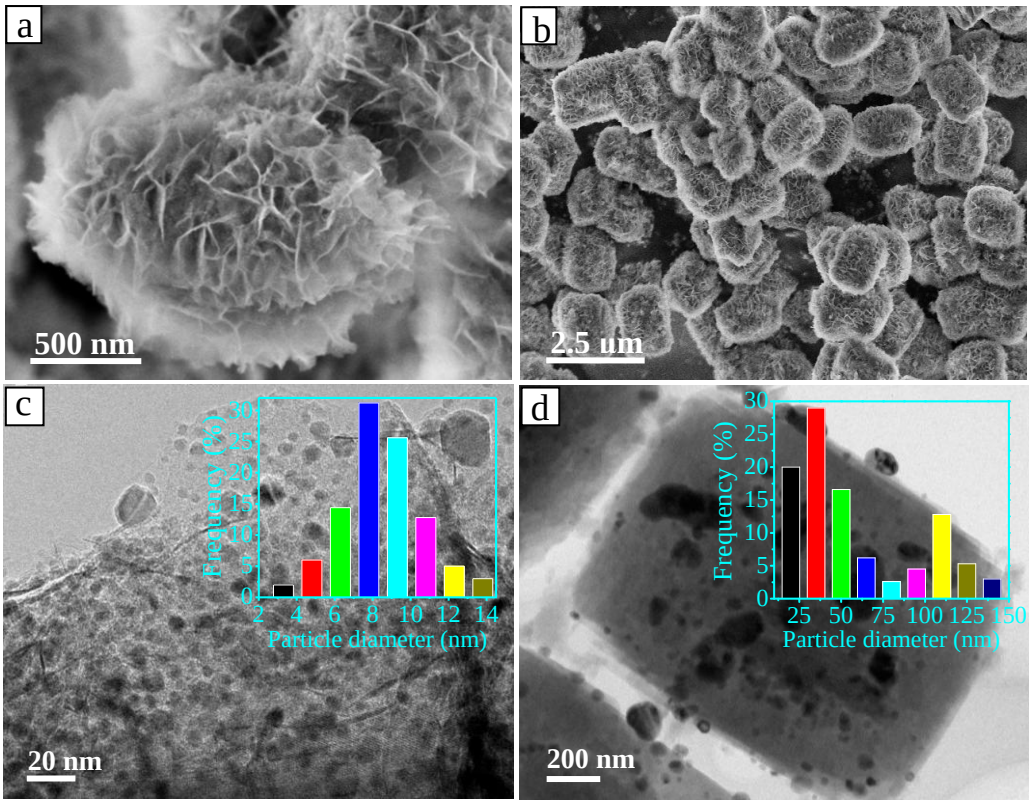

Fig. S18 SEM images of Ni/ZSM-5 (a, b) after four recycling runs, TEM images of Ni/ZSM-5 (c) and IM-Ni/ZSM-5 (d) after four recycling runs. The insets are the corresponding size distribution histogram of the Ni nanoparticles.

From the SEM images, we can see the morphology of the nanosheets on ZSM-5 did not change during the reaction. As shown in TEM images, the average diameters of Ni particles were still much smaller (around 7.7 nm), more importantly, these particles were more evenly distributed with a deviation of 1.6 nm. The much larger Ni particles in impregnated catalysts were further aggregated during the catalytic reaction; a large portion (about 25%) of strongly aggregated Ni particles (100 - 150 nm) was observed to coexist.

Moreover, According to the ICP analyses, we can calculate that the Ni content was 19.3 wt% and 15.6 wt% for Ni/ZSM-5 and IM-Ni/ZSM-5after four recycling runs, respectively.

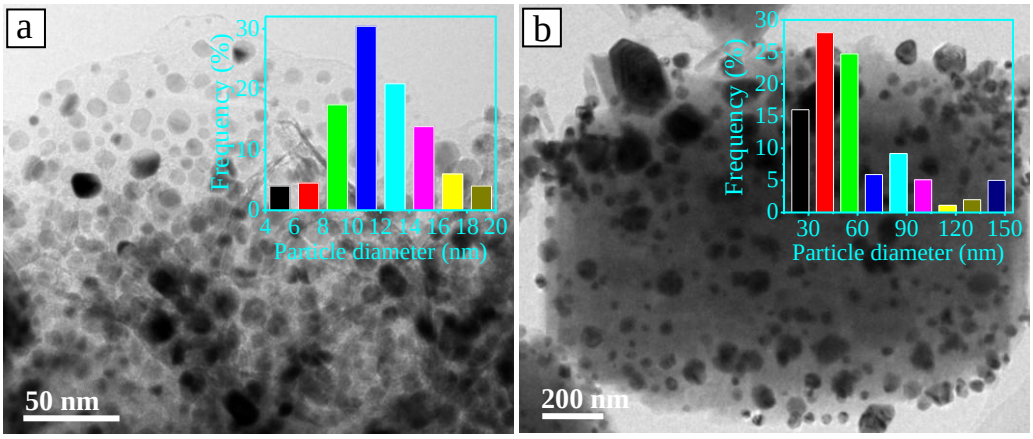

Fig. S19 TEM images of Ni/ZSM-5 (a) and IM-Ni/ZSM-5 (b) after high-temperature treatment at 800 ^{o}C for 24 h in a flow of H_2, insets are the corresponding size distribution histogram of the Ni nanoparticles.

The superior stability of Ni/ZSM-5 is mainly because of the confining effect of the mesoporous SiO_2 matrixes, which leads to anti-sintering during high-temperature treatment.

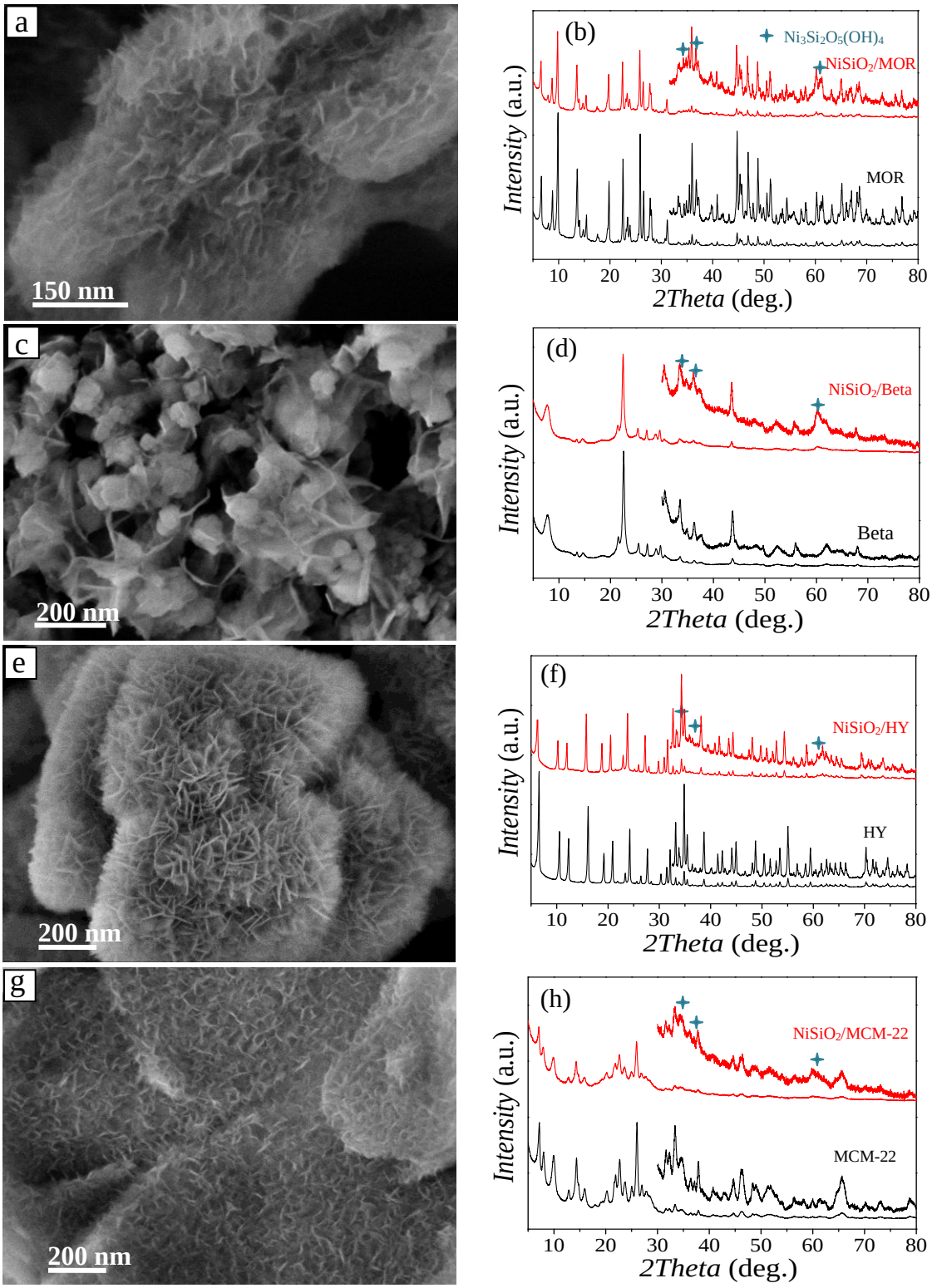

Fig. S20 SEM images of nickel silica coated on different zeolites: $NiSiO_2$/MOR (a), $NiSiO_2$/Beta (c), $NiSiO_2$/HY (e), $NiSiO_2$/MCM-22 (g). The corresponding XRD patterns were

given in (b), (d), (f) and (h), respectively. Black lines were pristine zeolites while red lines were $NiSiO_2$/Zeolites.

Notably, the Si/Al molar ratio for MOR, Beta, HY and MCM-22 used in the text were 40, 35, 28 and 42, respectively. When this novel method was transferred to other zeolites, high Si/Al molar ratio of zeolite would be the most important part .

Nickel silicate coated on different zeolites was synthesized by simply varying the types of zeolites added in the hydrothermal reaction solution. SEM images showed all zeolites were coated with flower-like nanosheets despite the different structures. Corresponding to the SEM images, XRD patterns of $NiSiO_2$/Zeolites showed the weak peaks indexed to nickel silicate ($Ni_3Si_2O_5(OH)_4$, JCPDS No. 49-1859), peaks centered at around 34.1^o, 36.7 ^{o} and 60.5^o were corresponded to the [200], [202] and [060] planes, respectively.

Moreover, comparison of stearic acid conversions on Ni/MOR, Ni/Beta, Ni/HY and Ni/MCM-22 can be seen in Table S4.

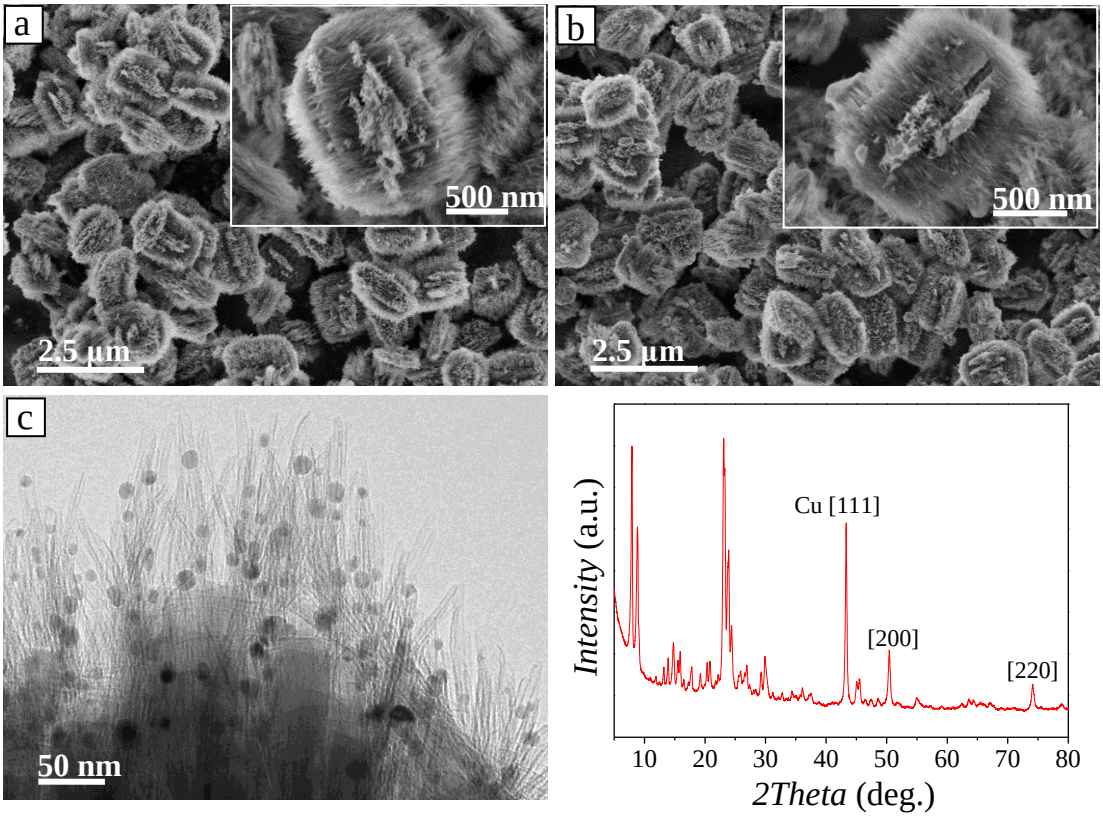

Fig. S21 SEM images of $CuSiO_2$/ZSM-5 (a) and Cu/ZSM-5 (b); high-resolution TEM image of Cu/SM-5 (c); XRD pattern of Cu/ZSM-5 (d).

After hydrothermal treatment in an alkaline solution containing copper ions at 150 ^oC for 3 h, the surface of $CuSiO_2$/ZSM-5 precursors is no longer smooth and composed of numerous needle-like nanotubes. After decomposition and reduction, Cu/ZSM-5 shows the similar morphology as $CuSiO_2$/ZSM-5. HRTEM image showed that Cu nanoparticles were uniformly dispersed on the nanotubes. In the XRD pattern of Cu/ZSM-5, the peaks centered at around 43.3^o, 50.4^o and 74.1^o corresponded to the [111], [200] and [220] planes of Cu.

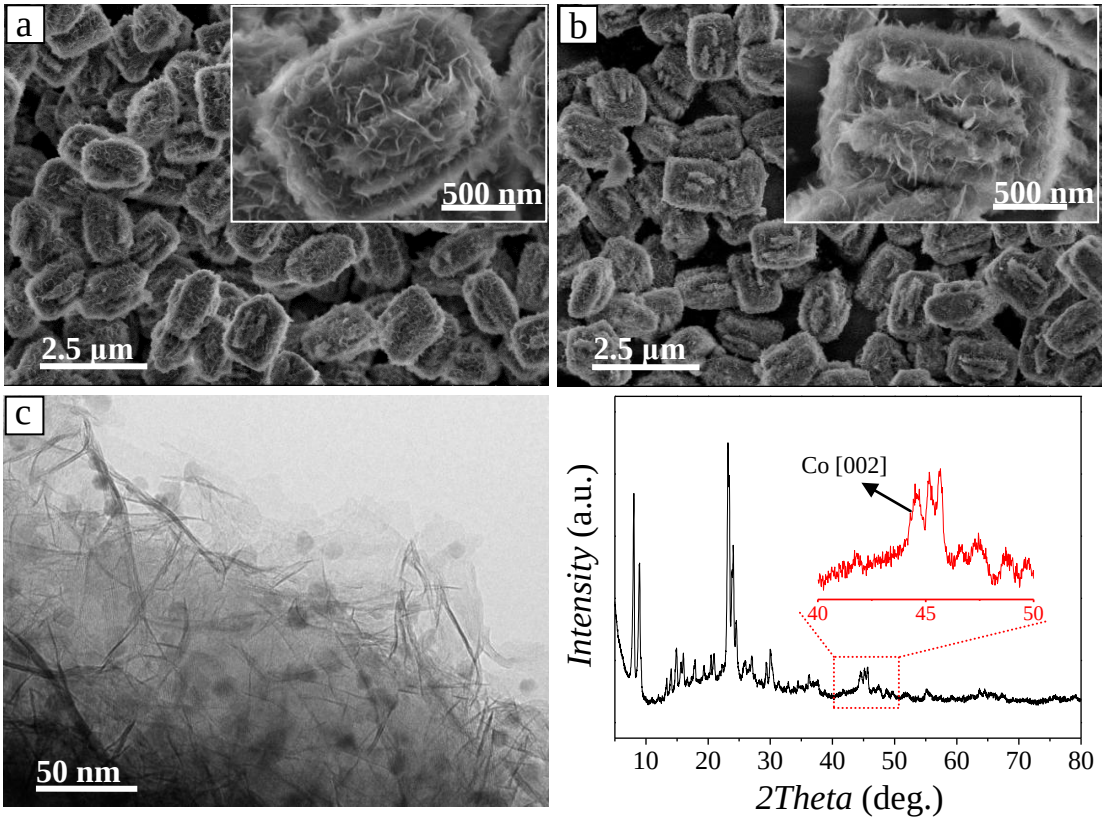

Fig. S22 SEM images of $CoSiO_2$/ZSM-5 (a) and Co/ZSM-5 (b); high-resolution TEM image of Co/SM-5 (c); XRD pattern of Co/ZSM-5 (d).

After similar hydrothermal treatment in an alkaline solution containing cobalt ions at 100 ^{o}C for 3 h, the surface of $CoSiO_2$/ZSM-5 precursors has a similar morphology to $NiSiO_2$/ZSM-5 (Fig. 1b) and is composed of flower-like nanosheets. After decomposition and reduction, Co/ZSM-5 still maintains the similar morphology as $CoSiO_2$/ZSM-5. HRTEM image showed Co nanoparticles were uniformly dispersed on the nanosheets. In XRD pattern of Co/ZSM-5, the weak peak centered at around 44.7 ^{o} corresponded to the [002] plane of Co.

Notes and references

1 D. Wang, L. Xu and P. Wu, *J. Mater. Chem., A,* 2014, **2**, 15535.

2 S. T. Gentry, S. F. Kendra and M. W. Bezpalko, *J. Phys, Chem., C,* 2011, **115**, 12736.

3 J. B. d'Espinose de la Caillerie, M. Kermarec and O. Clause, *J. Am. Chem. Soc*., 1995, **117**, 11471.

4 E. P. Parry, *J. Catal*., 1963, **2**, 371.